Journal of Membrane Science 485 (2015) 87–93

Contents lists available at ScienceDirect

Journal of Membrane Science

journal homepage: www.elsevier.com/locate/memsci

'Uphill' permeation of carbon dioxide across a composite molten salt-ceramic membrane

E.I. Papaioannou, H. Qi, I.S. Metcalfe *

School of Chemical Engineering and Advanced Materials, Newcastle University Merz Court, Newcastle upon Tyne NE1 7RU, UK

ARTICLE INFO

Article history:
Received 1 October 2014
Received in revised form
26 January 2015
Accepted 5 March 2015
Available online 14 March 2015

Keywords:
CO_2 separation
Composite molten salt-ceramic membranes
Uphill CO_2 permeation

ABSTRACT

Here, we show how a membrane can be designed and operated to achieve 'uphill' permeation of carbon dioxide against its own chemical potential difference by employing the transport of carbonate ions with coupled 'downhill' permeation of oxygen. Absolute values of the carbon dioxide permeability of the order of 10^6 Barrers are achieved experimentally over more than 200 h of operation. These permeabilities are some four orders of magnitude greater than polymeric gas separation membranes. We believe that these high permeabilities are due to the effective use of the oxygen chemical potential difference across the membrane as a driving force for carbonate transport.

1. Introduction

One approach to membrane design for selective carbon dioxide permeation is to fabricate a device consisting of two phases, one a carbonate-conducting mixture of molten alkali-metal carbonates and the other a predominantly electron-conducting solid phase [1]. The molten phase is held within the pores of the solid phase by capillary forces. On the feed side the carbonate forming reaction occurs:

$$CO_2 + \frac{1}{2}O_2 + 2e^- \rightarrow CO_3^{2-} \qquad \text{(Reaction1)}$$

Carbonate ions are transported across the membrane from the feed to the permeate side in the molten carbonate phase (Fig. 1). An equal and opposite flow of electrons (in terms of charge) passes through the solid phase. On the permeate side the reverse of Reaction [1] occurs liberating oxygen and carbon dioxide. Carbon dioxide and oxygen are effectively transported across the membrane simultaneously. The transport mechanism means that there is no fundamental trade-off between selectivity and permeability as in the case of polymeric membranes [2]. Thus both high selectivity and permeability in principle can be achieved. We investigate the permeability of a membrane consisting of a molten carbonate melt within an electron-conducting $La_{0.6}Sr_{0.4}Co_{0.2}Fe_{0.8}O_{3-\delta}$ host at 600 °C.

We note that this simultaneous transport of oxygen and carbon dioxide should allow us to permeate carbon dioxide against its own chemical potential difference. This of course does not violate thermodynamics as the chemical potential drop associated with the oxygen transport would need to be greater than the gain associated with carbon dioxide transport during permeation.

Uphill transport of carbon dioxide may be important for, e.g., post-combustion carbon dioxide capture processes. Flue gases are close to atmospheric pressure which means that if a high-mole-fraction carbon dioxide stream is to be produced compression is required. Uphill transport means that the chemical potential of oxygen in the flue gas stream can be harnessed to reduce compression costs.

Here we wish to clearly demonstrate uphill permeation so we select a rather high oxygen to carbon dioxide ratio in the feed-side inlet of 20:1 (an oxygen mole fraction of 20% and a carbon dioxide mole fraction of 1%). This oxygen to carbon dioxide ratio is much higher than would be found in a real flue gas. We permeate carbon dioxide from this feed stream into a permeate stream the inlet of composition of which contains 1% carbon dioxide but is oxygen free. In a practical membrane system one way of generating an appropriate permeate gas would be to take the feed-side outlet stream, split it, discharging the majority as treated flue gas, and remove oxygen from the remaining stream by e.g. passing it over a reduced oxygen carrier as part of a chemical looping combustion process [3]. This permeate stream would then essentially be oxygen free but with a carbon dioxide mole fraction equivalent to the membrane feed-side outlet mole fraction. Oxygen would need to be periodically removed from the permeate side by passing the stream over the oxygen carrier to ensure continued uphill permeation.

It is important to note that here, to obtain accurate permeation kinetics, we operate with good gas-phase mixing in both feed-side and permeate-side chambers. That is, the membrane is exposed to

* Corresponding author. Tel.: +44 191 208 5279.
E-mail address: i.metcalfe@newcastle.ac.uk (I.S. Metcalfe).

http://dx.doi.org/10.1016/j.memsci.2015.03.013

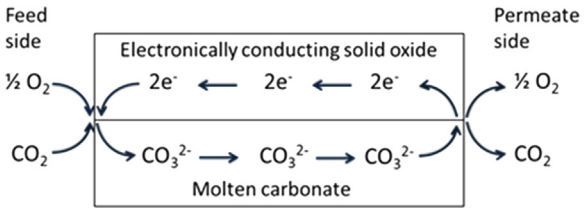

Fig. 1. Membrane transport mechanism.

uniform gas compositions on both sides of the membrane. The need to keep the membrane under a uniform gas composition necessitates the use of a relatively small membrane area. (The alternative would be to operate the membrane under conditions where there would be a significant change in gas composition on both sides between inlet and outlet. This mode of operation does not readily yield useful kinetic information.) We develop a robust methodology for determining permeation rates when the gas-phase component of interest (here carbon dioxide) is to be fed to both sides of the membrane. (Note that downhill permeation can easily be demonstrated by not feeding the component of interest to the permeate side. This is not true if one needs to prove uphill permeation.) This consists of dynamically following the outlet gas from both sides of a membrane with a similar mass spectrometers while switching between a symmetrical non-permeating condition and an asymmetrical permeating condition. The composition of the inlet permeate-side gas is not changed during this operation allowing accurate permeation rates to be determined from the change in the outlet composition of the permeate-side. Permeation rates are calculated from the difference in carbon dioxide mole fraction in the permeate-side outlet between an asymmetrical operating condition and a symmetrical operating condition. We believe that such a procedure leads to a more accurate determination of permeation rate, although admittedly under dynamic conditions, compared to more established methods in the literature (where the difference in composition between the outlet and inlet gases are used; the inlet gas composition being measured at some different time) as the composition change can be dynamically followed and the symmetrical operating condition provides a reference point. Furthermore the procedure can conclusively demonstrate the presence of uphill permeation. This dynamic permeation rate determination is complemented here by long term steady permeation rate determination.

2. Experimental

Commercial $La_{0.6}Sr_{0.4}Co_{0.2}Fe_{0.8}O_{3-\delta}$ (LSCF6428) powder was purchased from PRAXAIR. The powder was synthesised by combustion spray pyrolysis resulting in powders with particle size less than 1 μm. The pellets (20 mm diameter before sintering) were formed by uniaxially pressing approximately 1.5 g of the LSCF6428 powder mixed with 0.5 g corn starch (Sigma-Aldrich) at 3 *t* using an automatic ATLAS T25 press. Subsequently the pellets were sintered in air by ramping their temperature from room temperature to 200 °C at 60 °C h^{-1} and holding at 200 °C for 2 h (corn starch burn out and pore formation occurs at this temperature) and then ramping the temperature to 1250 °C at 60 °C h^{-1} and holding this temperature for 12 h (sintering occurs at this temperature) followed by cooling to room temperature at 60 °C h^{-1}. The diameter and the thickness of the sintered pellets were 14.6 mm and 1 mm approximately. Determining the mass of the pellets and using the bulk density of LSCF6428 of 6.08 g/cm^3 gives an approximate porosity of 26%. BET analysis gave a porosity of 32% with an average pore diameter of 4 μm. The total pore volume was approximately 0.1 cm^3.

Sintered LSCF6428 supports were infiltrated with molten carbonate (Alfa Aesar, 99% minimum purity) to obtain dual-phase membranes. Direct infiltration of the supports was performed using 0.2 g of a mixture of lithium carbonate (Li_2CO_3), sodium carbonate (Na_2CO_3) and potassium carbonate (K_2CO_3) in a molar ratio of 42.5/32.5/25. The membrane and carbonates were heated from room temperature to 500 °C at 300 °C h^{-1} followed by holding at 500 °C for 0.5 h to allow the molten carbonate to soak into the membrane via capillary action. The membrane was cooled to room temperature at 300 °C h^{-1} and its mass determined. Excess carbonates were present in the porous alumina vessel used to hold the membrane. Porosity in this vessel was essential to avoid adhesion of the membrane. The infiltration process was repeated until residual carbonates were seen to be present on the upper surface of the membrane (usually two steps in total). 0.08 g of carbonate was normally infiltrated into a pellet with pore volume of 0.1 cm^3 indicating that some gas may be trapped in the pore network on infiltration as the density of carbonates is 2 g cm^{-3} approximately [4]. The dual pellet membrane was then mounted on the top of an alumina tube using a high temperature commercial silver sealant (FuelCellMaterials, silver ink AG-1, 73.8 wt%). The sealant was allowed to dry in air for 6 h at room temperature (12 h at 75 °C for the long term permeation experiment). The final membrane area available for permeation was 0.5 cm^2 or 5×10^{-5} m^2. Each experiment was performed with a fresh membrane.

High temperature carbon dioxide permeation experiments were carried out in a permeation set-up operated at atmospheric pressure. The permeation cell comprises of two chambers, the feed-side chamber and the permeate-side chamber. The volumes of the feed-side and permeate-side chambers were 11.5 cm^3 and 250 cm^3 respectively. Residence time distributions (not shown) for both the feed- and permeate-side chambers indicated that there was a good degree of mixing on both sides and thus the membrane can be considered to be exposed to the outlet conditions.

The gases used, provided by BOC (certified gases, compositions on a molar basis), were 0.99% CO_2/1.03% N_2/19.45% O_2 in Ar (Cylinder 1, C-1), 1.03% CO_2 in Ar (Cylinder 2, C-2), 20% O_2 in Ar (Cylinder 3, C-3) and pure Ar (Cylinder 4, C-4). Nitrogen at approximately 1% in C-1 was introduced as a means to indicate inter-chamber leaks and in particular was chosen to be of a similar mole fraction to that of carbon dioxide in C-1 in order to estimate any carbon dioxide leak rates. It should be noted here that, unlike conventional 'down-hill' permeation, carbon dioxide leaks during an 'uphill' permeation experiment would lead to an underestimate in the flux and the approach is therefore fundamentally conservative in nature and much less likely to lead to misinterpretation.

The flows on both the feed and permeate sides were maintained at 20 cm^3 (STP)/min (1.49×10^{-5} mol s^{-1}). The outlet feed-side and permeate-side gases were analysed using two identical mass spectrometers (HIDEN, HALO 100-RC), MS-1 on the feed side and MS-2 on the permeate side. Both mass spectrometers were calibrated prior to the experiments and appeared to have linear responses for carbon dioxide mole fractions in the range of 0.5–1.5%. The carbon dioxide mole fractions measured were 0.97% for C-1 (using MS-1) and 1.04% for C-2 (using MS-2) immediately before Experiment 1. We see that MS-1 measures the carbon dioxide mole fraction as low by 0.02% while MS-2 measures high by 0.01%. In addition the resolution of the mass spectrometers is 0.01%.

For permeation experiments the membrane was heated in a temperature programmable furnace (VECSTAR VCTF-1) up to 600 °C at 120 °C h^{-1} and then held at 600 °C. Degassing of carbon dioxide was observed from about 400 °C. Outlet composition is presented once steady carbon dioxide levels were reached do not change more than ± 5% within 0.5 h.

Permeation rates are calculated for Experiment 1 and 2 from the difference in carbon dioxide mole fraction at steady state in the

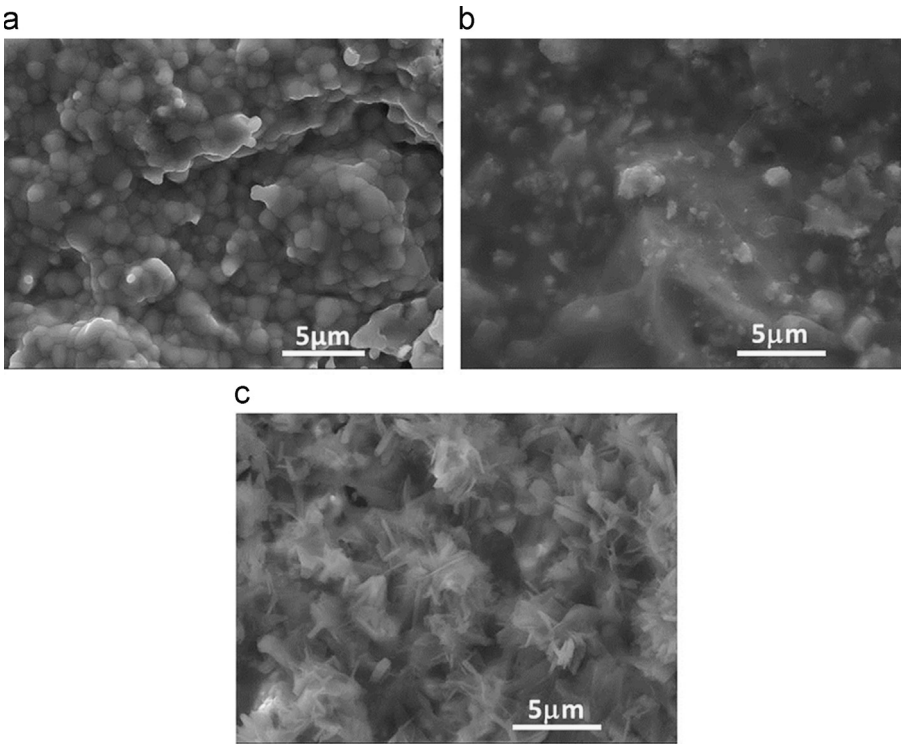

Fig. 2. SEM micrographs of the external surfaces of the LSCF6428 membrane (a) before infiltration with molten carbonate, (b) after infiltration with molten carbonate and (c) after permeation for 216 h.

permeate-side outlet between an asymmetrical operating condition (asym) and a symmetrical operating condition (sym). The permeate-side inlet gas composition is not changed during this process. Such a procedure should lead to a more accurate determination of permeation rate compared to more established methods in the literature (where the difference in composition between the outlet and inlet gases are used; the inlet gas composition often being measured at some very different time) as the composition change can be dynamically followed and the symmetrical operating condition provides a reference point. This procedure also minimises any problems with drift in the mass spectrometer signals.

To determine permeation rates the difference in permeate-side outlet mole fraction is multiplied by the molar flow rate on the permeate side, $\dot{n}''$,

Carbon dioxide permeation rate

$$= \left\{x''_{CO_2}(\text{outlet, asym}) - x''_{CO_2}(\text{outlet, sym})\right\}\dot{n}'' \quad (1)$$

Oxygen permeation rate

$$= \left\{x''_{O_2}(\text{outlet, asym}) - x''_{O_2}(\text{outlet, sym})\right\}\dot{n}'' \quad (2)$$

where x''_i is the mole fraction of component i and $''$ refers to the permeate side.

Fluxes are calculated by dividing the permeation rate by the active area of the membrane, A (5×10^{-5} m^2). Permeances are calculated by dividing the flux by the respective partial pressure driving force, that is the difference in mole fraction between the feed-side outlet gas and the permeate-side outlet gas under asymmetric conditions minus the difference in mole fraction between the feed-side outlet gas and the permeate-side outlet gas under symmetric conditions multiplied by the operating pressure, P.

$$\text{Carbon dioxide permeance} = \frac{\left\{x''_{CO_2}(\text{outlet, asym}) - x''_{CO_2}(\text{outlet, sym})\right\}\dot{n}''}{\left(\left\{x'_{CO_2}(\text{outlet, asym}) - x''_{CO_2}(\text{outlet, asym})\right\} - \left\{x'_{CO_2}(\text{outlet, sym}) - x''_{CO_2}(\text{outlet, sym})\right\}\right)P\cdot A} \quad (3)$$

$$\text{Oxygen permeance} = \frac{\left\{x''_{O_2}(\text{outlet, asym}) - x''_{O_2}(\text{outlet, sym})\right\}\dot{n}''}{\left(\left\{x'_{O_2}(\text{outlet, asym}) - x''_{O_2}(\text{outlet, asym})\right\} - \left\{x'_{O_2}(\text{outlet, sym}) - x''_{O_2}(\text{outlet, sym})\right\}\right)P\cdot A} \quad (4)$$

where ' refers to the feed-side. Once more by employing information about the switch between an asymmetrical operating condition (asym) and a symmetrical operating condition (sym) a more accurate driving force can be estimated.

Permeabilities are calculated by multiplying permeances by the membrane thickness of 10^{-3} m.

Feed side compositional changes can be used to perform a carbon dioxide balance. For Experiment 1 where the difference in symmetric and asymmetric feed-side carbon dioxide inlet mole fractions is only 0.04% a carbon dioxide material balance can be performed to show that the rate of consumption of carbon dioxide on the feed side matches the rate of carbon dioxide evolution on the permeate side within measurement uncertainty.

Experiments with carbon dioxide and inert alone and oxygen and inert alone were also performed at 600 °C to test whether the carbon dioxide can permeate across the membrane in the absence of gas phase oxygen or oxygen can permeate across the membrane in the absence of gas phase carbon dioxide.

3. Results and discussion

3.1. Membrane characterisation

The morphology, microstructure, phase structure and elemental analysis of the membrane were characterised by a scanning electron microscope (SEM) and energy dispersive X-ray spectroscopy (EDS) (Rontec Quantax 1.2 FEI XL30 ESEM-FEG) and X-ray diffraction (XRD) (PANalytical Empyrean Diffractometer operated in reflection mode, CuKα). It is important to note that these techniques were not employed in-situ and the carbonate is in the solid state at the time of characterisation.

SEM micrographs of the external surfaces of the LSCF6428 membrane before infiltration with molten carbonate, after infiltration with molten carbonate and after permeation for 216 h were recorded. There were no significant differences between feed-side and permeate-side SEMs so here we only show feed-side images. Fig. 2(a) shows the membrane before infiltration. Fig. 2(b) shows the membrane after infiltration but before any permeation (fresh membrane). Fig. 2(c) shows the membrane after 216 h of continuous permeation (used membrane). EDS analysis (not shown) of the infiltrated membrane (fresh and used) indicated the presence of sodium and potassium over the entire surfaces of the membrane (lithium is too light to be detected). A discernible change is observed between the fresh membrane and the used membrane which after long term operation shows elongated carbonate crystals.

XRD diffractograms of the fresh and used membrane are shown in Fig. 3. Data were acquired for 2θ values from 20° to 80° at a step size 0.017° with a dwell time of 1 s. Both diffractograms show a fully developed perovskite-like structure and peaks indicative of molten carbonate at 2θ values of 29.4° and 37.3° [5]. Note that the relative intensity of the molten carbonate peaks is quite low compared to the LSCF peaks and that carbonate peak intensity drops after permeation. Both of these findings were also observed in [5]. Some additional peaks may be due to the formation of interfacial species.

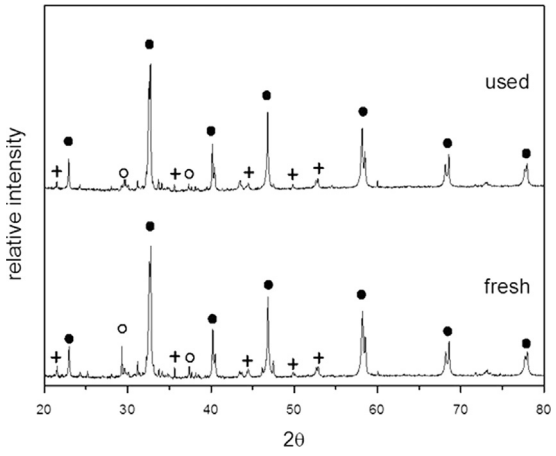

Fig. 3. XRD diffractograms of the fresh and used membrane. Both diffractograms show a fully developed perovskite-like structure (indicated by •) and peaks indicative of molten carbonate (indicated by ○). Some additional peaks may be due to the formation of interfacial species (indicated by +).

3.2. CO_2 'uphill' permeation

In Experiment 1, the membrane is initially under symmetrical conditions with gas from cylinder C-2 (1.03% CO_2 in Ar) fed to both sides of the membrane (as indicated by 'sym$_1$' in Fig. 4(a)). Both sides are at atmospheric pressure. At steady state the carbon dioxide mole fraction in the outlet from the feed side is measured to be 1.02% while the carbon dioxide mole fraction in the outlet from the permeate side is 1.06%. This is consistent with no permeation or degassing of carbon dioxide given the characteristics of the gas analysis.

After introducing the gas from cylinder C-1 (0.99% CO_2/1.03% N_2/19.45% O_2 in Ar) to the feed-side inlet (at time t_1) the carbon dioxide outlet mole fractions reach values of 0.91% and 1.12% in feed and permeate side, respectively, at time t_2. (Note that the decrease in the carbon dioxide mole fraction in the feed-side outlet appears to be greater than the increase in the permeate-side outlet. However, this is not the case as the feed-side inlet suffered a 0.04% decrease in carbon dioxide inlet mole fraction on gas switching.) Interestingly the carbon dioxide outlet mole fraction on the feed side seems to undershoot its steady value while the mole fraction on the permeate side overshoots its steady value. This could be due to the carbon dioxide flux being initially higher than its steady value as no oxygen is fed to the permeate side, rather the oxygen mole fraction on the permeate side needs to establish itself as a consequence of permeation. However, the time constant for mixing in the permeate side chamber (around 0.07 h) is rather short compared to the nature of the transient behaviour. We know that the composition and behaviour of molten carbonates can be complex [6] and it is possible that the composition of the melt is also changing during these transients. In addition there appears to be some nitrogen evolution on the feed side. The nitrogen evolution may be due to a loss of occluded gas from, e.g., the pore network.

0.91% carbon dioxide is below the inlet carbon dioxide mole fraction on the feed side; 1.12% is above the inlet carbon dioxide mole fraction on the permeate side. This difference in mole fraction cannot be attributed to measurement uncertainty and/or systematic errors in the mass spectrometer readings (a systematic 0.03% difference in the mass spectrometer readings at this mole fraction for this experiment and a resolution of 0.01%). We conclude that uphill carbon dioxide permeation is taking place at this time.

At time t_2 there is 0.15% oxygen in the permeate-side outlet. This is higher than would be expected if oxygen was only present on the permeate side as a result of carbonate permeation (note that oxygen in the absence of carbon dioxide cannot permeate across the membrane – see later description of Experiment 4). It may be possible that carbonate in the melt decomposes releasing carbon dioxide back into the feed side gas while oxygen is transported to the permeate side (Reaction [2]), i.e. after decomposition both carbon dioxide and oxygen are transported under their own individual chemical potential gradients.

$$CO_3^{2-}(\text{melt}) \rightarrow CO_2(\text{feed side}) + \frac{1}{2}O_2(\text{permeate side}) + 2e^- \quad \text{(Reaction2)}$$

This would require other mobile species to be present within the melt such as neutral carbon dioxide or oxygen ions.

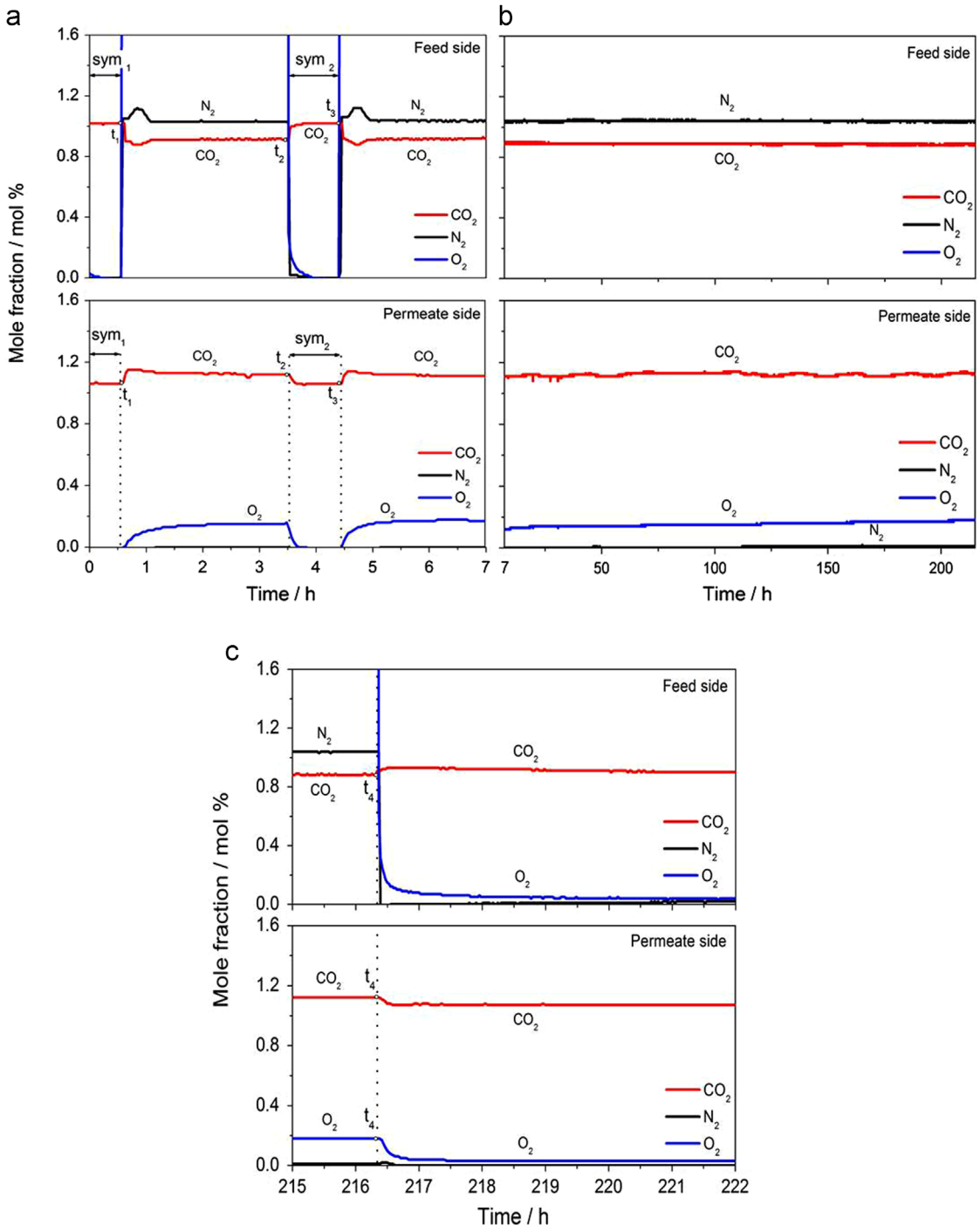

Fig. 4. Mole fractions of gases in both feed- and permeate-side outlets for Experiment 1 at 600 °C. (a) During asymmetrical operation: feed-side inlet: 0.99% CO_2/1.03% N_2/19.45% O_2 in Ar, permeate-side inlet: 1.03% CO_2 in Ar. During symmetrical operation: feed- and permeate side inlets: 1.03% CO_2 in Ar. A flux of $1.8 \pm 0.3 \times 10^{-4}$ mol m^{-2} s^{-1} is determined at time t_3. (b) Uphill permeation is performed over 216 h (different timescales are used) during asymmetrical operation with no apparent drop in flux or appearance of a trans-membrane leak and (c) return to symmetrical operation. Note that the value for the oxygen mole fraction in the feed-side outlet during asymmetric operation is off scale.

At time t_2 we return to a symmetrical condition with steady mole fractions achieved at time t_3. We use the permeate-side outlet mole fractions at times t_2 and t_3 to calculate a carbon dioxide permeation rate of $9 \pm 2 \times 10^{-9}$ mol s^{-1} or flux of $1.8 \pm 0.3 \times 10^{-4}$ mol m^{-2} s^{-1} at time t_3. We use the permeation rate from this experiment to determine a carbon dioxide permeance of -1.1×10^{-6} mol m^{-2} s^{-1} Pa^{-1} (the permeance is negative as the carbon dioxide permeation is against the carbon dioxide partial pressure difference of -170 Pa between feed and permeate sides; the mole fraction difference is -0.17%).

Experiment 1 is then repeated with a fresh membrane. Uphill permeation is performed over 216 h (Fig. 4(b)). There is no apparent drop in flux or appearance of a trans-membrane leak (i.e. nitrogen on the permeate side) over this time period (very slight variations in the outlet permeate-side carbon dioxide mole fraction can be seen; such variation are associated with temperature changes in the laboratory over a 24 h period). There does appear to be a very gradual increase in the rate of oxygen permeation. At time t_4 (Fig. 4(c)) the measured carbon dioxide outlet mole fractions reach values of 0.89% and 1.12% in feed and permeate

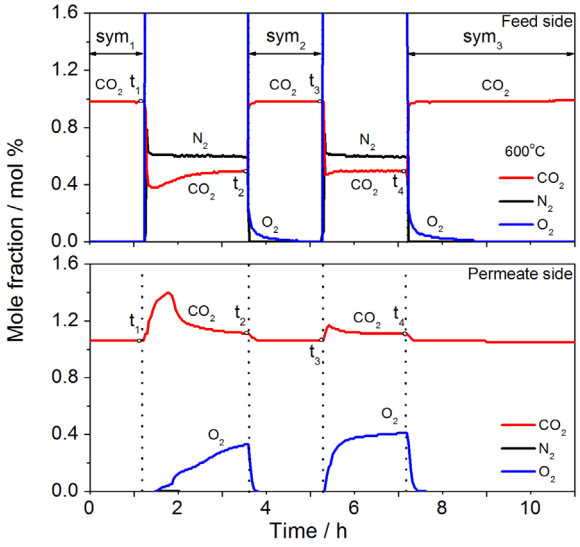

Fig. 5. Mole fractions of gases in both feed- and permeate-side outlets for Experiment 2 at 600 ºC. During symmetrical operation: feed- and permeate-side inlets: 1.03% CO_2 in Ar. During asymmetrical operation: feed-side inlet: 0.51% CO_2/0.57% N_2/19.45% O_2 in Ar, permeate-side inlet: 1.03% CO_2 in Ar. A flux of $1.5 \pm 0.3 \times 10^{-4}$ mol m^{-2} s^{-1} is determined at time t_4. Note that the value for the oxygen mole fraction in the feed-side outlet during asymmetric operation is off scale.

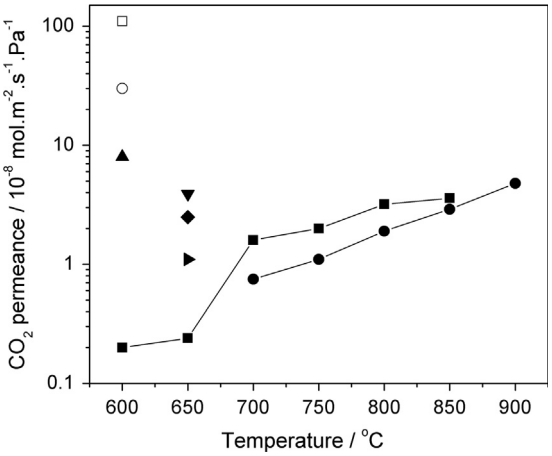

Fig. 6. Carbon dioxide permeances (logarithmic scale) for references: [1] (◆), [4] (▼), [5] (●), [7] (■), [8] (▶), [9] (▲) as a function of temperature. For reference [5] a range of solid phases were investigated; here only the permeances of the best performing system (a YSZ solid phase) are shown. The absolute values of the permeances determined in Experiment 1 (□) and 2 (○) are used.

side, respectively, and the permeation rate is similar to that determined by the transient experiment described above. After time t_4 we return to a symmetrical condition by supplying gas from cylinder C-2 to both sides. Over the 216 h period the molar amount of carbon dioxide permeated is one order of magnitude greater than the molar hold up of carbonate in the membrane (the membrane contains 0.08 g of carbonate at an average molecular weight of 100 g mol^{-1} or 8×10^{-4} mol of carbonate compared to a permeation rate of $\sim 10^{-8}$ mol s^{-1} over 8×10^5 s or 8×10^{-3} mol of carbon dioxide) proving that carbonate decomposition cannot be obscuring the results.

At the start of Experiment 2 (Fig. 5) the membrane was again initially under symmetrical conditions ('sym_1') with the C-2 gas (1.03% CO_2 in Ar) as the feed to both sides. At time t_1 the inlet to the feed side is switched to an approximately 1:1 M ratio mixture of the gases from C-1 (0.99% CO_2/1.03% N_2/19.45% O_2 in Ar) and C-3 (20% O_2 in Ar) in such a way that the carbon dioxide mole fraction was 0.51%. The oxygen mole fraction remained at 20% and the nitrogen mole fraction was measured to be 0.57%. Note the transient large carbon dioxide mole fraction difference across the membrane about 0.5 h after time t_1 consistent with a much higher transient uphill permeation rate. At time t_2 symmetrical conditions are again adopted ('sym_2'), held for approximately two hours and at t_3 the system again is exposed to the previous asymmetrical operating conditions. Steady permeation appears to be achieved after about one hour. We use the data at times t_3 and t_4 to calculate the carbon dioxide permeation rate. The difference in carbon dioxide mole fraction between the permeate side (unchanged inlet gas composition) outlet at time t_3 and time t_4 yields a flux of carbon dioxide of $1.5 \pm 0.3 \times 10^{-4}$ mol m^{-2} s^{-1} at time t_4. Here it is clear that carbon dioxide is permeating from a mole fraction of around 0.5% to around 1.0%. At time t_4 there is 0.41% oxygen in the permeate-side outlet. Again this is much higher than would be expected if a stoichiometric amount of oxygen permeated across the membrane. The carbon dioxide partial pressure driving force is close to -520 Pa giving a carbon dioxide permeance of -3×10^{-7} mol m^{-2} s^{-1} Pa^{-1}.

The absolute value of these carbon dioxide permeances are at least one order of magnitude greater than the previously determined permeance of a carbonate and electron-conducting membrane [2] at a similar temperature and the permeances determined by other workers employing carbonate and ion-conducting membranes [6] (Fig. 6) although Zhang et al. appear to have achieved excellent permeance by optimising the pore structure of the solid phase [9]. We ascribe these high permeances as being due to the membrane's ability to harness the chemical potential difference of the oxygen to drive carbon dioxide permeation. If we evaluate oxygen permeances then the values achieved are, as expected, similar to those of other workers. In Experiment 1 we determine an oxygen permeance of 2.3×10^{-8} mol m^{-2} s^{-1} Pa^{-1} at time t_2 while in Experiment 2 we determine an oxygen permeance of 6.3×10^{-8} mol m^{-2} s^{-1} Pa^{-1} at time t_4 in a similar range to the permeances observed by other authors (Fig. 6).

Absolute values of carbon dioxide permeabilities can be calculated for the above experiments (1 Barrer $= 3.348 \times 10^{-16}$ mol mm^{-2} s^{-1} Pa^{-1}) using the membrane thickness of 10^{-3} m. The absolute values of these permeabilities are 3×10^6 Barrers and 9×10^5 Barrers. If we compare these permeabilities and separation factor to those of polymeric membranes [2] we can see that the membranes under consideration here have permeablilities that are almost four orders of magnitude greater than polymeric systems with similar carbon dioxide-nitrogen separation factors. The absence of nitrogen permeation means that we can estimate the maximum possible nitrogen permeation rate and hence a separation factor. Combined with the driving force for nitrogen permeation we obtain an absolute value of the ratio of the carbon dioxide permeance to the nitrogen permeance (the separation factor) of 40 or greater.

To test whether carbon dioxide can permeate across the membrane in the absence of gas phase oxygen as a result of the diffusion of neutral carbon dioxide the following experiment was performed (Experiment 3). At the start of Experiment 3 the membrane was held under symmetrical conditions with the gas from C-2 (1.03% CO_2 in Ar) as the feed to both sides ('sym_1' in Fig. 7). In Fig. 7 we can follow the mole fractions of carbon dioxide and oxygen in both the feed-side and permeate-side outlets. The feed to the permeate side is switched, at time t_1, to a carbon dioxide mole fraction of approximately 0.6%. Carbon dioxide permeation (determined from feed-side consumption of carbon dioxide in this case using data at times t_1 and t_2) appeared to occur at the very limit of resolution i.e. a flux of approximately 3×10^{-5} mol m^{-2} s^{-1}.

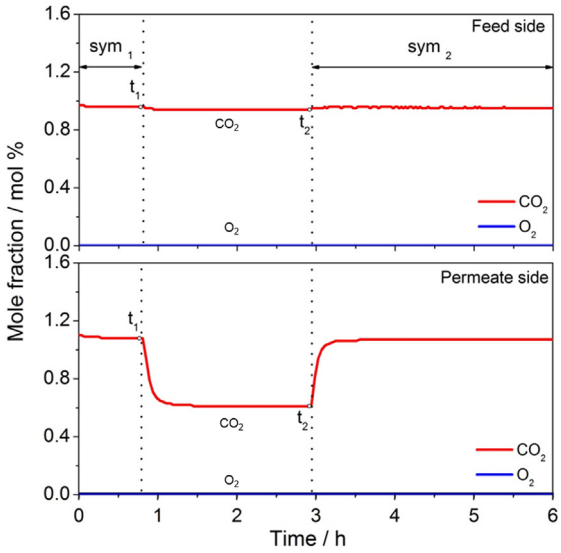

Fig. 7. Mole fractions of gases in both feed- and permeate-side outlets for Experiment 3 at 600 °C. During symmetrical operation: feed- and permeate-side: 1.03% CO_2 in Ar. During asymmetrical operation: feed-side inlet: 1.03% CO_2 in Ar, permeate-side inlet: approximately 0.6% CO_2 in Ar.

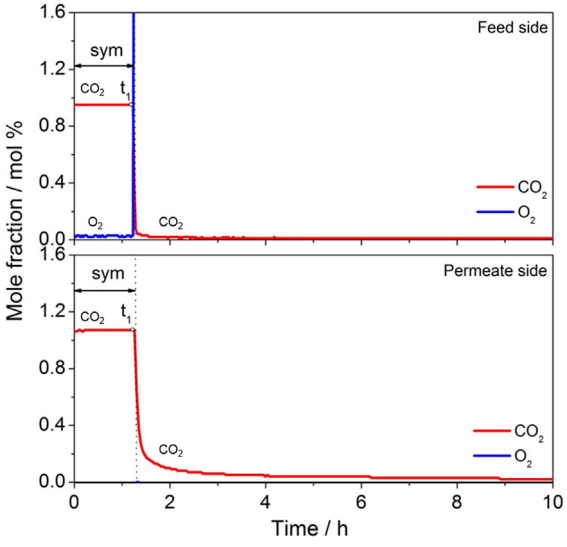

Fig. 8. Mole fractions of gases in both feed- and permeate-side outlets for Experiment 4 at 600 °C. During symmetrical operation: feed- and permeate-side: 1.03% CO_2 in Ar. During asymmetrical operation: feed-side inlet: 20% O_2 in Ar, permeate-side inlet: pure Ar. Note that the value for the oxygen mole fraction in the feed-side outlet during asymmetric operation is off scale.

To test whether oxygen could permeate across the membrane in the absence of carbon dioxide Experiment 4 was performed. At the start of Experiment 4 the membrane was held under symmetrical conditions with C-2 gas (1.03% CO_2 in Ar) as the feed to both sides ('sym' in Fig. 8). At time t_1, the feed-side inlet is switched to C-3 (20% O_2 in Ar) and the permeate-side inlet to C-4 (pure Ar). Oxygen can be seen in the feed-side outlet. No oxygen appears in the permeate-side outlet and we conclude that there is no measurable oxygen permeation. Carbon dioxide in the permeate-side outlet (interestingly there is much less loss of carbon dioxide into the feed side perhaps because of the presence of a large amount of oxygen) may be due to a combination of gas-phase mixing and degassing from, i.e., changing composition of, the molten carbonate.

4. Conclusions

In conclusion, we have shown for the first time how a membrane can be used to permeate carbon dioxide against its own chemical potential difference. Such uphill permeation may be important for e.g. future carbon dioxide capture processes. The membrane operation relies upon dual carbonate and electronic conduction for selectivity and the fact that the loss in oxygen chemical potential on carbonate permeation is greater than the gain in carbon dioxide chemical potential for uphill permeation. Membrane permeabilities of the order of 10^6 Barrers were achieved at 600 °C. Membrane performance is stable over more than 200 h of operation.

Acknowledgement

We wish to thank Dr. Alan Thursfield with help setting up preliminary experiments. We thank Jianwei Lu for operating the membrane system during the 216 h experiment. We thank Dr. Zhentao Wu and Professor Kang Li of Imperial College for the BET analysis and Dr. Dragos Neagu and Professor John Irvine of St Andrews University for the XRD analysis. The research leading to these results has received funding from the European Research Council under the European Union's Seventh Framework Programme (FP/2007-2013)/ERC Grant Agreement number 320725 and from the EPSRC via a PLATFORM Grant, EP/G012865/1.

References

[1] S.J. Chung, J.H. Park, D. Li, J.I. Ida, J.Y.S. Lin, Dual-phase metal-carbonate membrane for high-temperature carbon dioxide separation, Ind. Eng. Chem. Res. 44 (2005) 7999–8006.
[2] L.M. Robeson, The upper bound revisited, J. Membr. Sci. 320 (2005) 390–400.
[3] L.S. Fan, F.X. Li, Chemical looping technology and its fossil energy conversion applications, Ind. Eng. Chem. Res. 49 (2010) 10200–10211.
[4] B. Lu, Y.S. Lin, Synthesis and characterisation of thin ceramic-carbonate dual-phase membranes for carbon dioxide separation, J. Membr. Sci. 444 (2013) 402–411.
[5] M. Anderson, Y.S. Lin, Carbonate-ceramic dual-phase membrane for carbon dioxide separation, J. Membr. Sci. 357 (2010) 122–129.
[6] P. Tomczyk, M. Mosialek, Investigation of the oxygen electrode reaction in basic molten carbonates using electrochemical impedance spectroscopy, Electrochim. Acta 46 (2001) 3023–3032.
[7] J.L. Wade, C. Lee, A.C. West, K.S. Lackner, Composite electrolyte membranes for high temperature CO_2 separation, J. Membr. Sci. 369 (2011) 20–29.
[8] Z.B. Rui, M. Anderson, Y.D. Li, Y.S. Lin, Ionic conducting ceramic and carbonate dual phase membranes for carbon dioxide separation, J. Membr. Sci. 417 (2012) 174–182.
[9] L.L. Zhang, N.S. Xu, X. Li, S.W. Wang, K. Huang, W.H. Harris, W.K. Chiu, High CO_2 permeation flux enabled by highly interconnected three-dimensional ionic channels in selective CO_2 separation membranes, Energy Environ. Sci. 5 (2012) 8310–8317.